Sanna Mönkölä

Applications of Discrete Exterior Calculus

From Physical Modeling to High-Performance Computing

Work done in the research group on Computational Field Theory
with Mikael Myyrä, Joona Räty, Markus Kivioja, Sampsa Kiiskinen,
Jonni Lohi, Jukka Räbinä, Tytti Saksa, Tuomo Rossi, and Lauri Kettunen

Faculty of Information Technology
University of Jyväskylä, Finland

UNIVERSITY OF JYVÄSKYLÄ
FACULTY OF INFORMATION TECHNOLOGY

Outline

1. Model
    - First-order presentation
2. Computational grids
3. DEC discretization
4. Application areas
    - DEC in space + time-stepping
    - Time-harmonic problems
    - Parallelization
    - Spacetime discretization
    - Higher-order discretization
5. Summary

Models

Generalization in four-dimensional spacetime

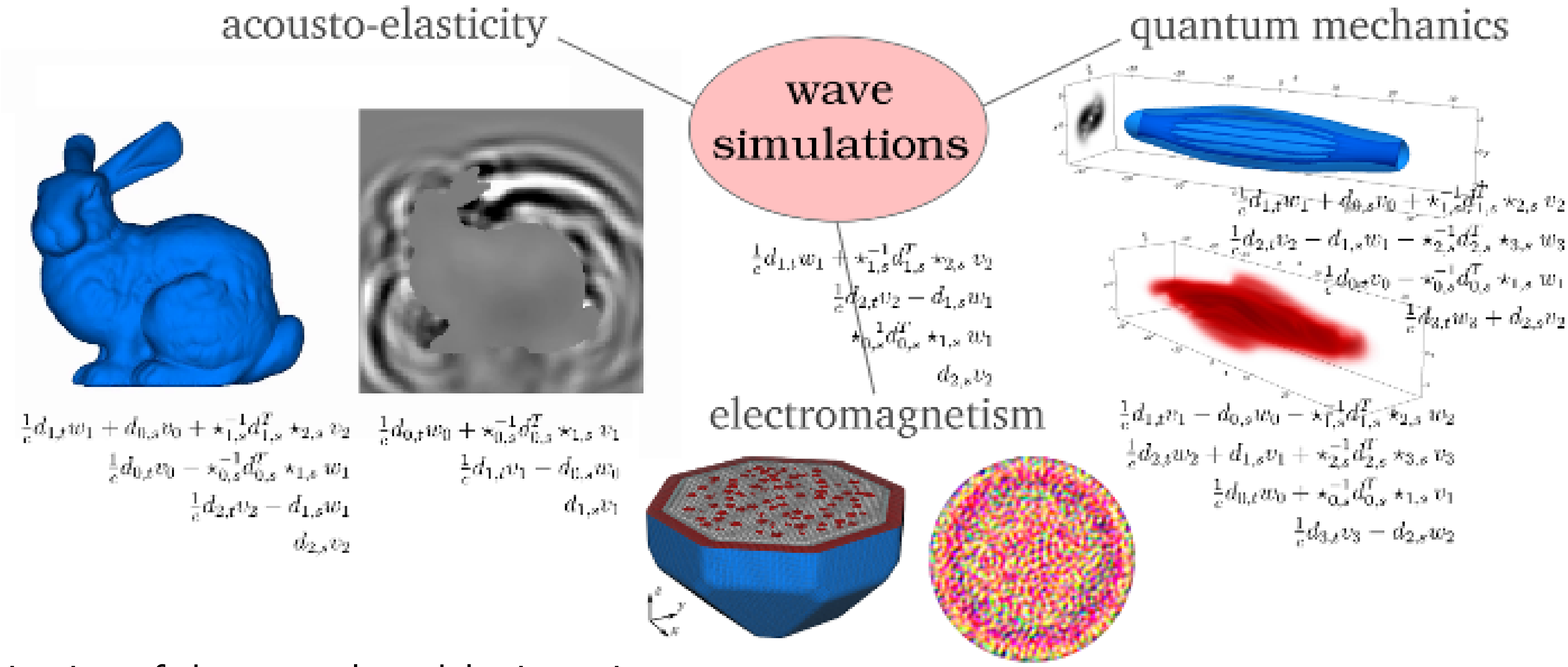

Derivation of the general model; viewpoints:

- Geometric algebra in Minkowski spacetime $\mathbb{R}^{1,d}$, differential of the general multivector/multiform[*].
- The conservation laws derived from the least action principle[†], the action is set up by Hamilton's principal function of the form $S = \frac{1}{2}\int_\Omega (dF \wedge \star dF) = \frac{1}{2}\int_\Omega \langle dF, dF\rangle\, vol$.

[*] *S. Mönkölä, J. Räbinä, T. Saksa, and T. Rossi. (2+ 1)-dimensional discrete exterior discretization of a general wave model in Minkowski spacetime. Results in Applied Mathematics, 25, 100528, 2025.*

[†] *L. Kettunen, S. Mönkölä, J. Parkkonen, and T. Rossi. Systematic Imposition of Partial Differential Equations in Boundary Value Problems. In Impact of Scientific Computing on Science and Society, 25–44, Springer, 2023.*

General differential form formulation in 4D

The differentials dx^0, dx^1, dx^2 and dx^3 are basis 1-forms and basis k-forms are constructed as wedge (exterior) products of k basis 1-forms, such that, $dx^i \wedge dx^i = 0$ and $dx^i \wedge dx^j = -dx^j \wedge dx^i$.

With differential (multi)forms $\tilde{F}$ and $\tilde{J}$ we can present the wave equations as

$$\boxed{\boldsymbol{\partial} \tilde{F} = \tilde{J},} \qquad \boxed{\boldsymbol{\partial} \star \tilde{F} = \star \tilde{J},}$$

where

$$\begin{aligned}\tilde{F} = {} & \tilde{f}_1 + \tilde{f}_2 dx^0 + \tilde{f}_3 dx^1 + \tilde{f}_4 dx^2 + \tilde{f}_5 dx^3 + \tilde{f}_6(dx^0 \wedge dx^1) + \tilde{f}_7(dx^0 \wedge dx^2) + \tilde{f}_8(dx^0 \wedge dx^3) + \tilde{f}_{11}(dx^2 \wedge dx^3) + \tilde{f}_{10}(dx^3 \wedge dx^1)\\ & + \tilde{f}_9(dx^1 \wedge dx^2) + \tilde{f}_{14}(dx^0 \wedge dx^2 \wedge dx^3) + \tilde{f}_{13}(dx^0 \wedge dx^3 \wedge dx^1) + \tilde{f}_{12}(dx^0 \wedge dx^1 \wedge dx^2) + \tilde{f}_{15}(dx^1 \wedge dx^2 \wedge dx^3)\\ & + \tilde{f}_{16}(dx^0 \wedge dx^1 \wedge dx^2 \wedge dx^3),\end{aligned}$$

$$\begin{aligned}\tilde{J} = {} & \tilde{b}_1 + \tilde{b}_2 dx^0 + \tilde{b}_3 dx^1 + \tilde{b}_4 dx^2 + \tilde{b}_5 dx^3 + \tilde{b}_6(dx^0 \wedge dx^1) + \tilde{b}_7(dx^0 \wedge dx^2) + \tilde{b}_8(dx^0 \wedge dx^3) + \tilde{b}_{11}(dx^2 \wedge dx^3) + \tilde{b}_{10}(dx^3 \wedge dx^1)\\ & + \tilde{b}_9(dx^1 \wedge dx^2) + \tilde{b}_{14}(dx^0 \wedge dx^2 \wedge dx^3) + \tilde{b}_{13}(dx^0 \wedge dx^3 \wedge dx^1) + \tilde{b}_{12}(dx^0 \wedge dx^1 \wedge dx^2) + \tilde{b}_{15}(dx^1 \wedge dx^2 \wedge dx^3)\\ & + \tilde{b}_{16}(dx^0 \wedge dx^1 \wedge dx^2 \wedge dx^3),\end{aligned}$$

and $\boldsymbol{\partial} = (\boldsymbol{d} + \boldsymbol{\delta})$ is the differential operator that is the sum of the exterior derivative $\boldsymbol{d}$ and its coderivative (interior derivative) $\boldsymbol{\delta} = (-1)^k \star^{-1} \boldsymbol{d} \star$, and $\star$ is the Hodge star operator.

Computational grids

Domain Ω as a cell complex

- Consists of differentiable k-cells (k-manifolds with boundary).

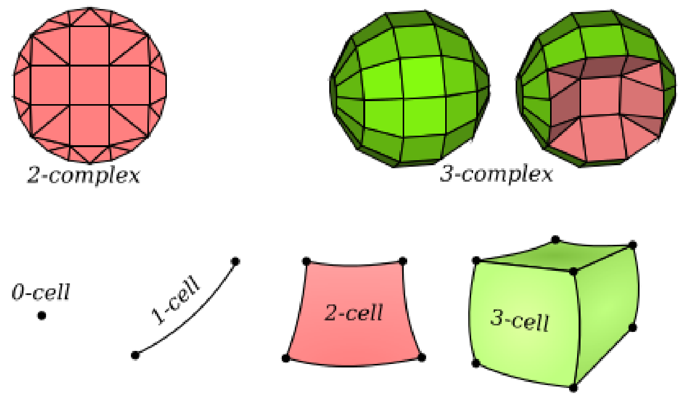

Partly structured grids

- Convex polyhedral elements; cubes, prisms, pyramids, octahedra . . .

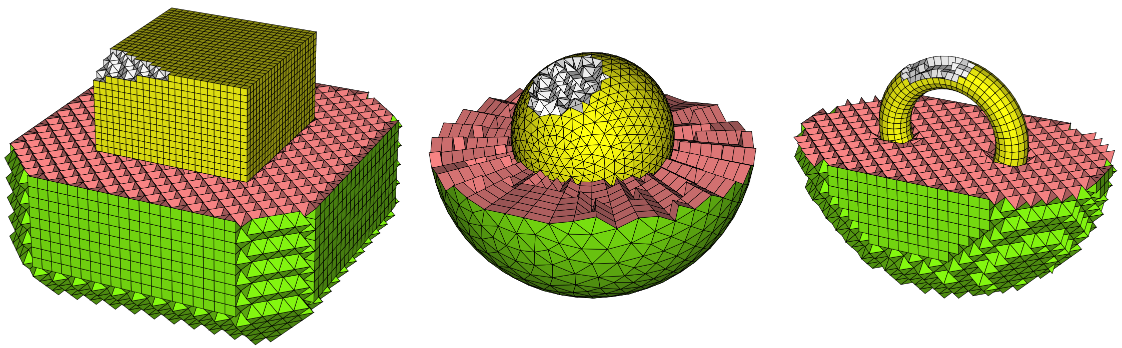

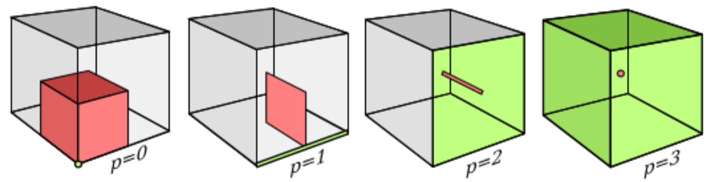

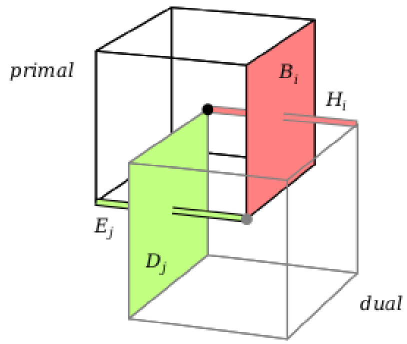

Orthogonality of the primal and dual mesh elements

- Weighted circumcenters (Voronoi diagram).

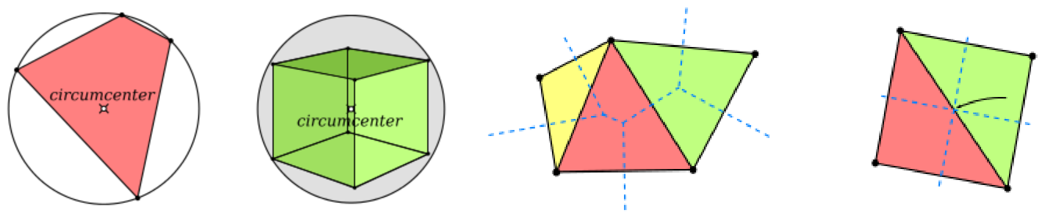

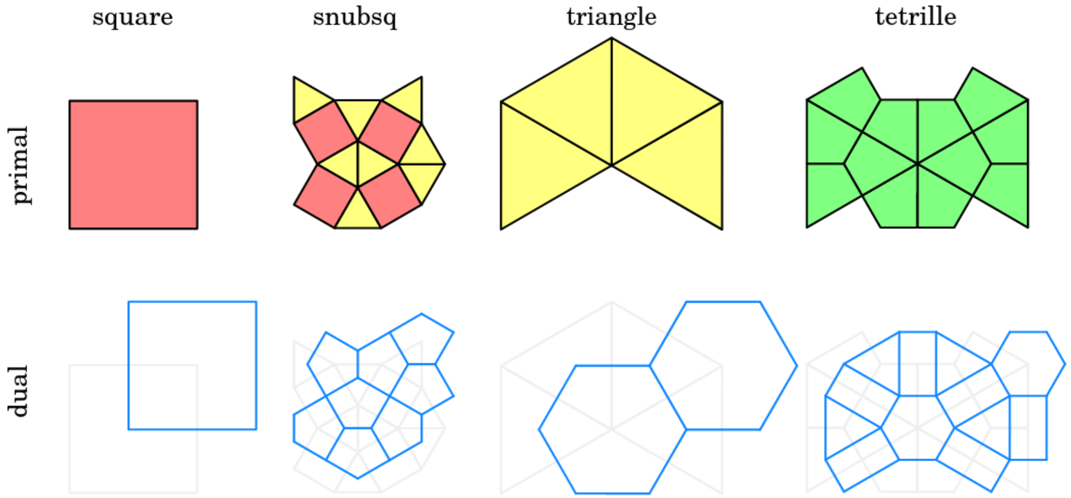

2D spatial grids (Euclidean metric).

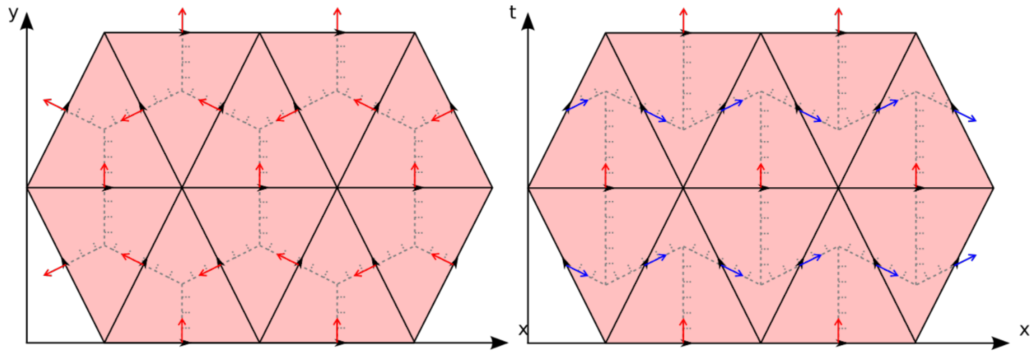

Euclidean vs. Minkowski metric (2D grids).

Each k-cell is associated with a corresponding dual $(n-k)$-cell.

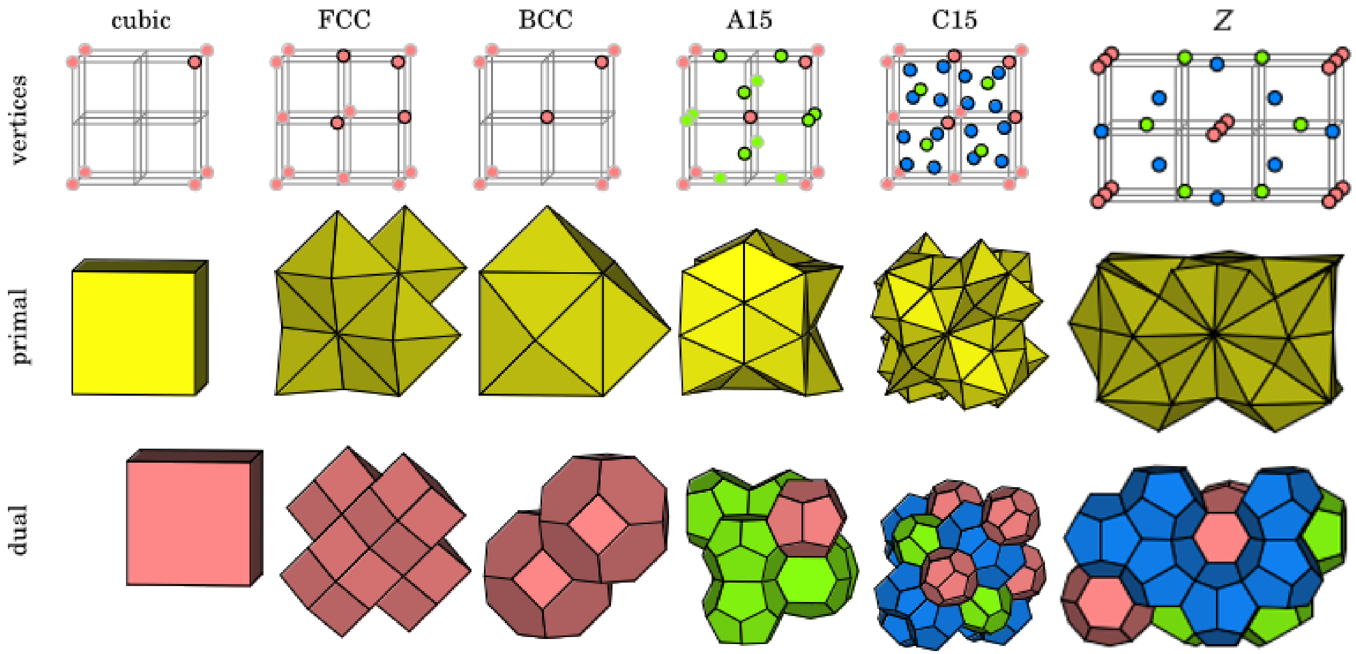

3D spatial grids (Euclidean metric).

J. Räbinä L. Kettunen, S. Mönkölä, and T. Rossi. Generalized wave propagation problems and discrete exterior calculus. ESAIM: Mathematical Modelling and Numerical Analysis, 52(3):1195–1218, 2018.

J. Räbinä, S. Mönkölä, and T. Rossi. Efficient Time Integration of Maxwell's Equations with Generalized Finite Differences. SIAM Journal on Scientific Computing, 37(6), B834–B854, 2015.

Discrete exterior calculus*

*M. Desbrun, A. N. Hirani, J. E. Marsden. Discrete exterior calculus for variational problems in computer vision and graphics. In 42nd IEEE International Conference on Decision and Control, vol. 5, 4902–4907, 2003.

Spacetime discretization

- Extension of the exterior calculus to discrete spaces – generalization of the FDTD.
- Vectors of degrees of freedom associated with primal and dual grid components.
- Variables can be associated with nodes (0-forms), edges (1-forms), faces (2-forms), volumes (3-forms), hypervolumes (4-forms).

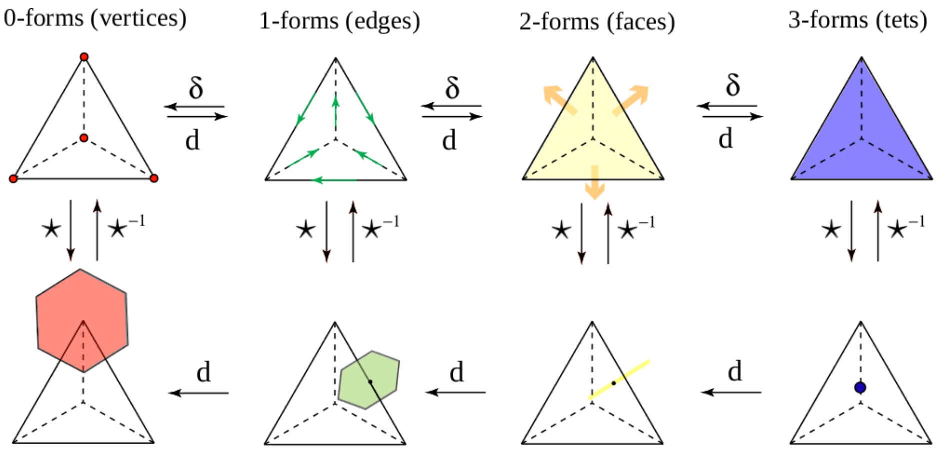

M. Desbrun, E. Kanso, Y. Tong. Discrete differential forms for computational modeling. In Discrete differential geometry, Birkhäuser Basel, 287–324, 2008.

- Discrete k-form corresponding to a differential form α_k is $u_k = \int_{\mathcal{C}_k} \alpha_k = \begin{pmatrix} \int_{\mathcal{C}_{k1}} \alpha_k \\ \vdots \\ \int_{\mathcal{C}_{kn_p}} \alpha_k \end{pmatrix}$, where $\mathcal{C}_{ki}$ is the ith k-cell and n_p is the number of k-cell.

- **Exterior derivative** d (generalization of grad, div, curl) and the corresponding **codifferential** δ.
  - Incidence matrix d_k operates discrete differential k-forms u_k and represents the neighboring relations and *relative orientations*.It is exact because the Stokes theorem holds exactly; $d_k u_k = d_k \int_{C_k} \alpha_k = \int_{C_{k+1}} d\alpha_k$.

- The **Hodge operator** $\star$ maps a differential k-form to a differential $(n-k)$-form.
  - The discrete Hodge operator $\star_k$ is a matrix *mapping between the primal and dual mesh* (diagonal if the dual elements are orthogonal to the primal elements).

Discrete k-forms, incidence matrices d_k, and the corresponding co-operators δ_k (include discrete Hodge operators) with spatial (subscript s) and temporal (subscript t) components.

Generalized model in four dimensions without external forces

$$\left(\begin{array}{c|cc|cc|cc|c}
 & \delta_{0s} & \frac{1}{\Delta t^2} d_{0t} & & & & & \\
\hline
d_{0s} & & & \delta_{1s} & \frac{1}{\Delta t^2} d_{1t} & & & \\
d_{0t} & & & & -\delta_{0s} & & & \\
\hline
 & d_{1s} & & & & \delta_{2s} & \frac{1}{\Delta t^2} d_{2t} & \\
 & d_{1t} & -d_{0s} & & & & -\delta_{1s} & \\
\hline
 & & & d_{2s} & & & & \frac{1}{\Delta t^2} d_{3t} \\
 & & & d_{2t} & -d_{1s} & & & -\delta_{2s} \\
\hline
 & & & & & d_{3t} & -d_{2s} &
\end{array}\right)
\left(\begin{array}{c}
u_{0s} \\ \hline u_{1s} \\ u_{1t} \\ \hline u_{2s} \\ u_{2t} \\ \hline u_{3s} \\ u_{3t} \\ \hline u_{4t}
\end{array}\right) = 0. \tag{1}$$

Leads to a leapfrog style timestepping.

Computational tools

PyDEC [a]

Comparison DEC vs. FEEC [b]
Exact controllability method
for time-harmonic problems

[a] https://github.com/hirani/pydec
[b] https://doi.org/10.1016/j.cam.2024.116154

Developed at the University of Jyväskylä:

Core library (C++)[a]
CPU parallelism (OpenMP, MPI)
Mesh generator (space, spacetime)
Classical & quantum mechanics

[a] https://sites.google.com/jyu.fi/gfd/
https://github.com/juolrabi/gfd

GPU acceleration (CUDA) [a]
Quantum models:
Gross–Pitaevskii, BEC,
knots, skyrmions, Alice rings

[a] https://github.com/markus-kivioja/GpuDecGpe

On-going implementation (Rust)[a]
Nanoscale thermal transport
Plasmas (Maxwell–Vlasov)

[a] https://codeberg.org/molentum/dexterior

Higher-order DEC[a]
Whitney/cubical forms
Sparse non-diagonal Hodge

[a] https://github.com/higher-order-dec

Application areas

Photonic crystals

$$B^{n+\frac{1}{2}} = B^{n-\frac{1}{2}} - \Delta t(\mathbf{d}_0 E^n - J_H^n)$$
$$E^{n+1} = E^n + \Delta t \star_{\varepsilon}^{-1}(\mathbf{d}_0^T \star_{\nu} B^{n+\frac{1}{2}} + J_E^{n+\frac{1}{2}})$$

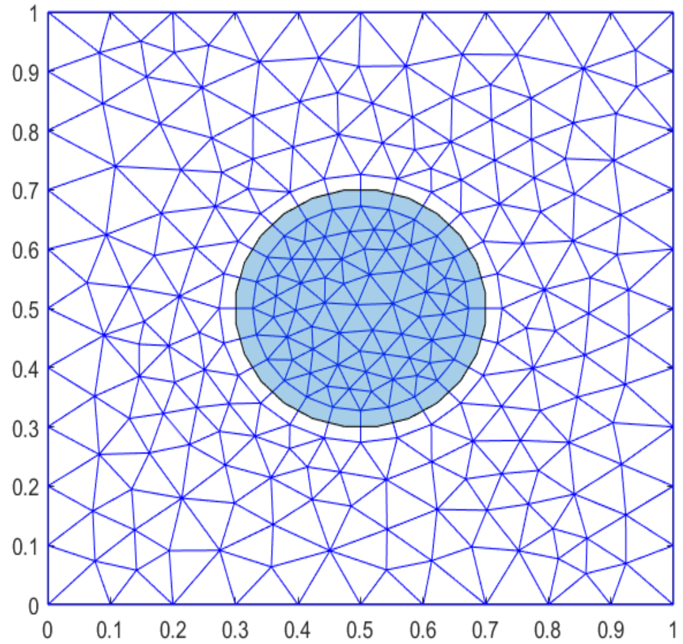

2D nanoscale electromagnetics with leap-frog time-stepping

- 15×7 periodic cells with the rods in the middle row removed
- a narrow width modified Gaussian pulse source,
- photonic band gap at frequency 0.4.

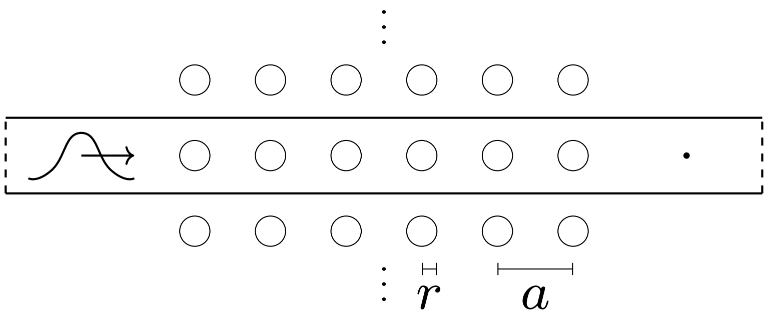

$\varepsilon = 8.9$
$\mu = 1$
$r = 0.2$
$a = 1$

$h_{\max} = 1/32$
$h_{\min} \approx 0.4 h_{\max}$

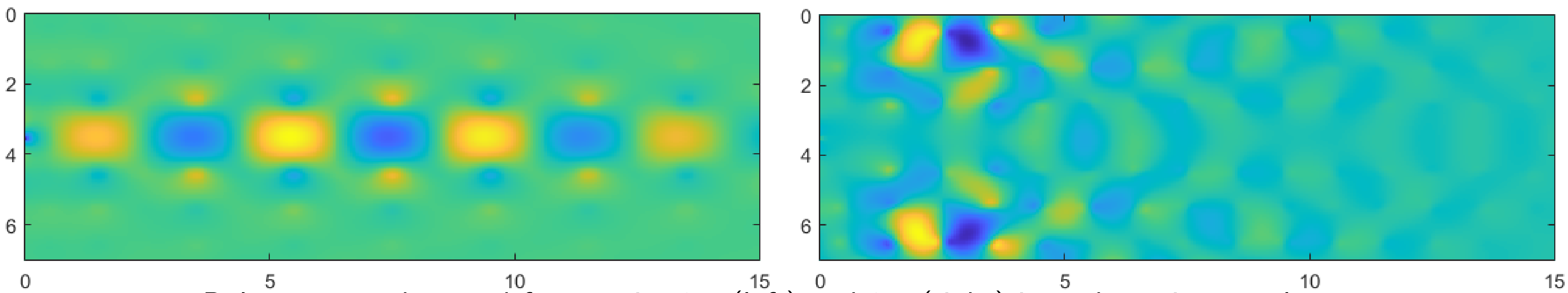

Pulses centered around frequencies 0.4 (left) and 0.5 (right) in a photonic crystal array

S. Mönkölä, and J. Räty. Discrete exterior calculus for photonic crystal waveguides. International Journal for Numerical Methods in Engineering, 124(5), 1035–1054, 2023.

Double slit experiment

- Schrödinger equation for free particle $i\hbar\frac{\partial}{\partial t}\Psi = -\frac{\hbar^2}{2m}\nabla^2\Psi$
- We separate complex valued wave function into real and imaginary components $\Psi = A + iB$ (0-forms A and B)

$$\partial_t A + \delta_0 d_0 B = 0,$$
$$\partial_t B - \delta_0 d_0 A = 0.$$

- We perform double slit experiment with 8 million unknowns.

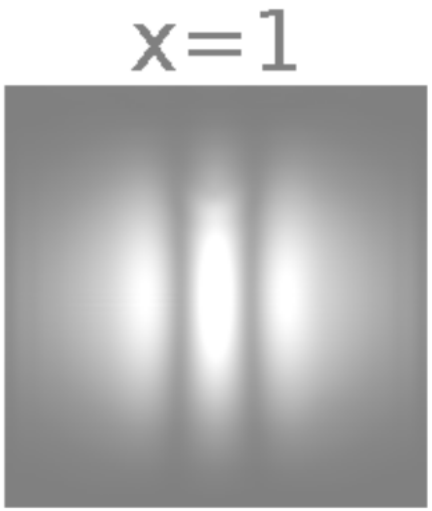

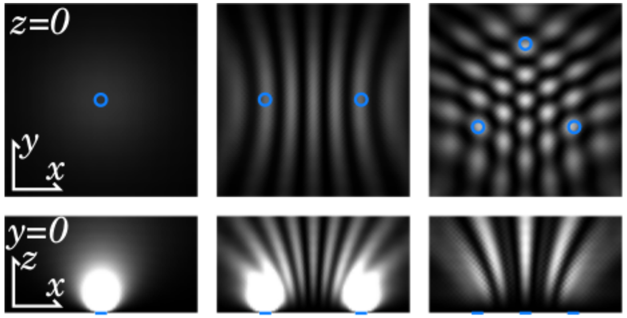

https://sites.google.com/jyu.fi/gfd/applications/quantum-mechanics

Training a convolutional neural network with electromagnetic simulations

- Simulated light propagation.
  - Time-harmonic source term.
  - Number of elements per wavelength 100–150.
  - Time integration until steady state is reached (**asymptotic approach**).
  - The solution is integrated to obtain reflectance for given frequency.

$$-\star_\mu \, \partial_t \mathbf{h} = \mathrm{d}\mathbf{e},$$
$$(\star_\epsilon \partial_t + \star_\sigma)\,\mathbf{e} = \mathrm{d}^{\mathsf{T}}\mathbf{h},$$

- An inverse model based on convolutional neural networks analyzing thin-film layer thicknesses from hyperspectral images (400–1000 nm wavelength range).
  - Training: 72000 DEC simulations for each film material.

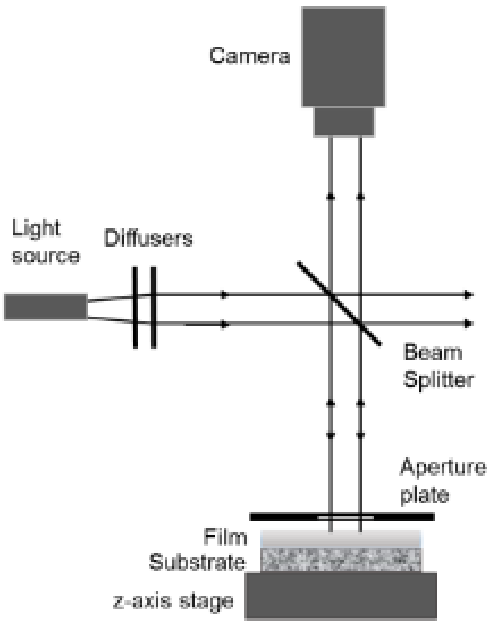

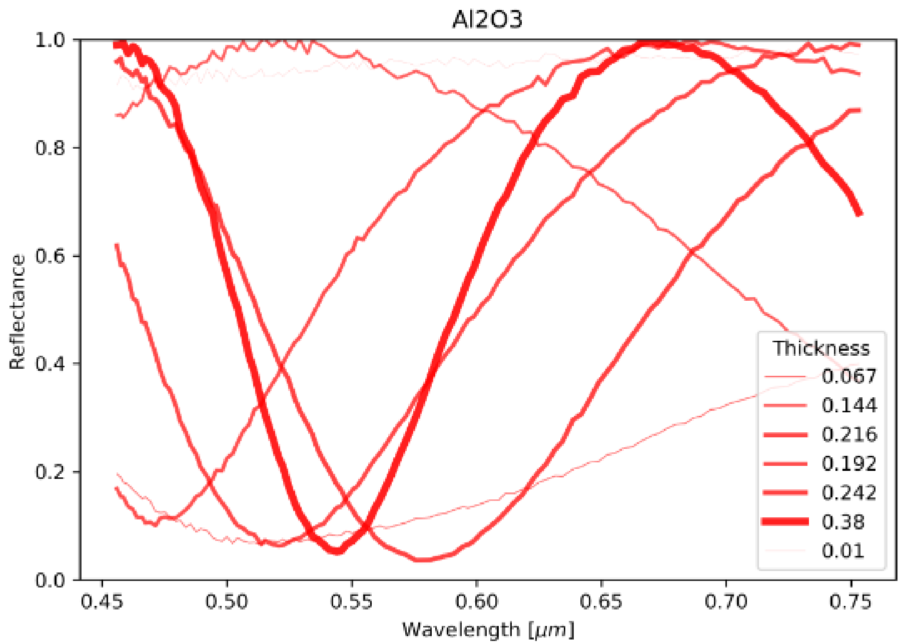

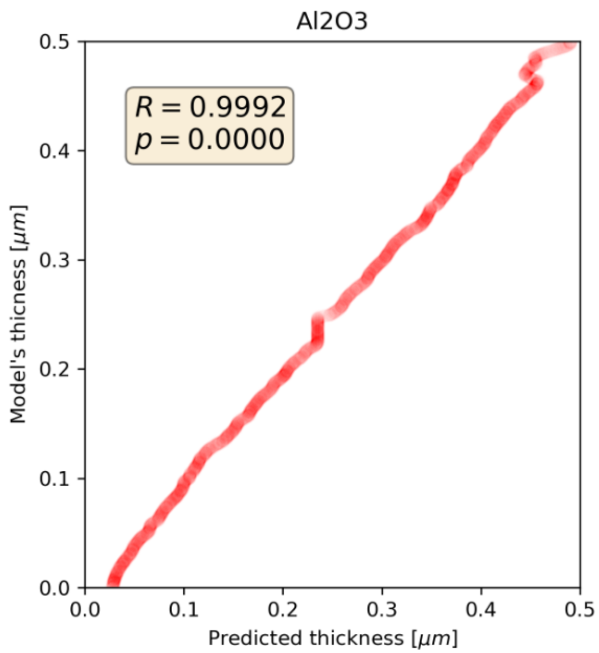

A-L. Erkkilä, J. Räbinä, I. Pölönen, T. Sajavaara, E. Alakoski, and T. Tuovinen. Using wave propagation simulations and convolutional neural networks to retrieve thin film thickness from hyperspectral images. In Computational Sciences and Artificial Intelligence in Industry, 261–275, Springer, 2021.

Exact controllability approach for time-harmonic problems [†] [‡]

- Accelerates the convergence of the **asymptotic approach** by minimizing the problem related energy (controlled time integration).

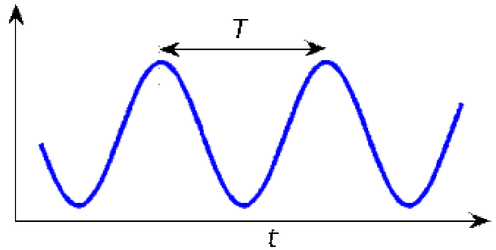

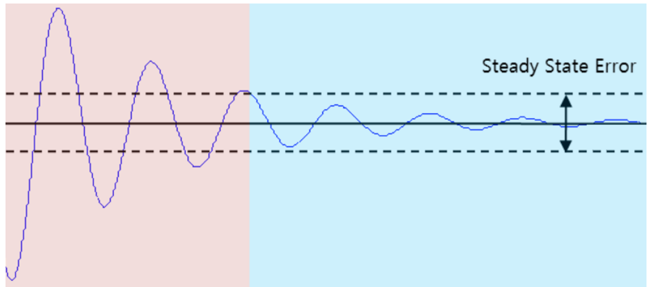

  - A variation of the asymptotic approach with periodic constraints: the residual of the algorithm defines at each iteration how far the solution is from a periodic one and accelerates the convergence rate by giving an impulse to the system.

  - Energy for electromagnetic scattering problem is of the form $\mathcal{E}(E, H) = \frac{1}{2}\left(E^T \star_\epsilon \; E + H^T \star_\mu \; H\right)$.

  - The time-harmonic solution can be found by minimizing $\mathcal{E}(E - \mathbf{E}_0, H - \mathbf{H}_0)$, where the initial conditions $\mathbf{E}_0$ and $\mathbf{H}_0$ are also the control variables.

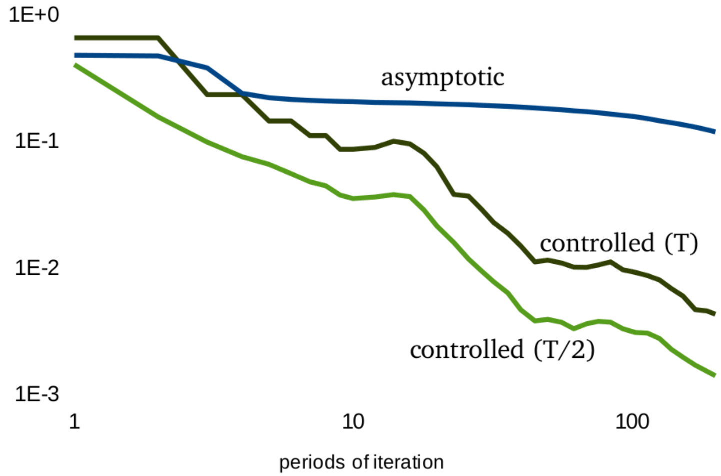

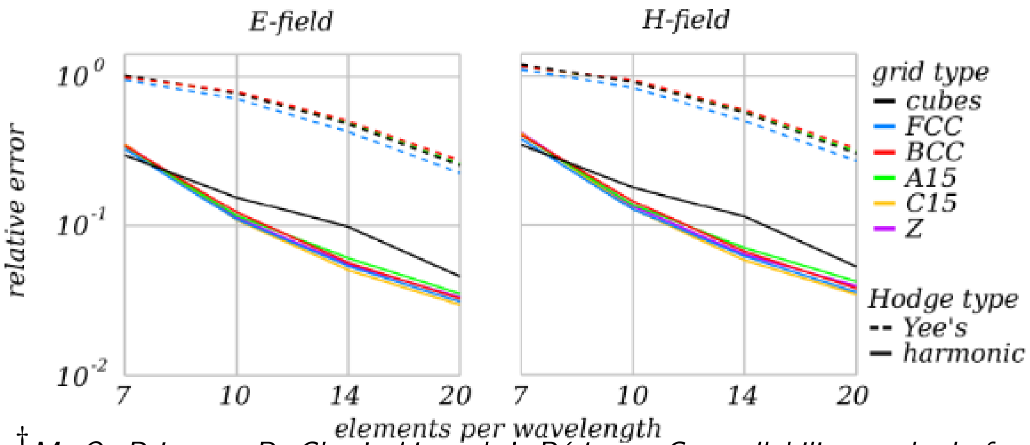

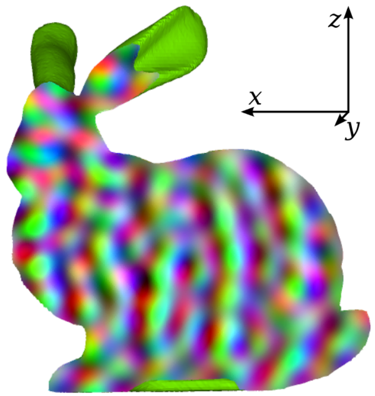

[†] M. O. Bristeau, R. Glowinski, and J. Périaux. *Controllability methods for the computation of time-periodic solutions; application to scattering. Journal of Computational Physics, 147(2), 265–292, 1998.*

[‡] S. Mönkölä, J. Räbinä, and T. Rossi. *Time-harmonic electromagnetics with exact controllability and discrete exterior calculus. Comptes Rendus. Mécanique, 351(S1), 647–665, 2023.*

Exact controllability: examples of acoustics

- For the same level of accuracy, DEC provides a lower computational cost than FEEC. [§]
- Efficient for scattering problems with non-convex objects. [¶]

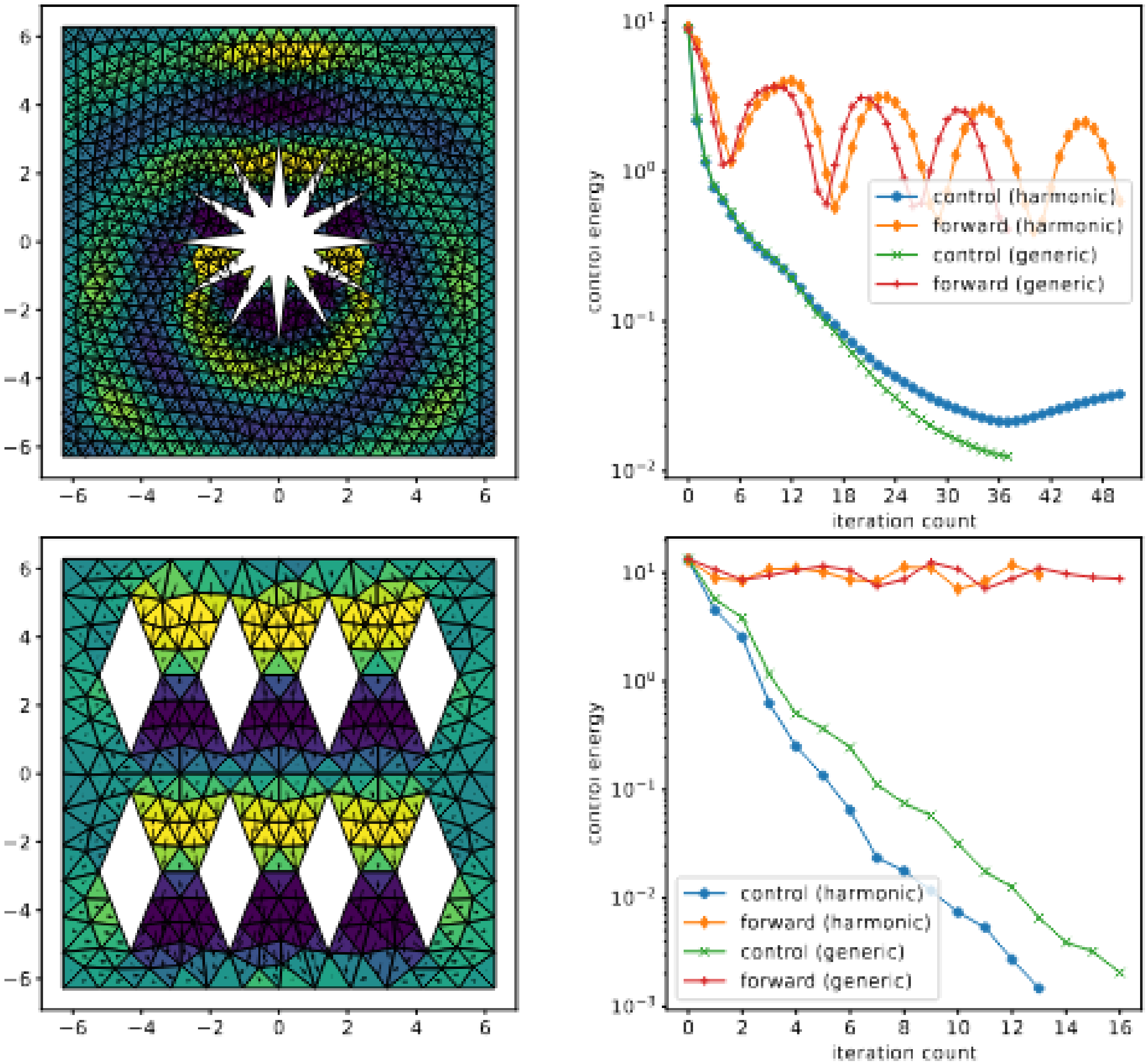

[§] *T. Saksa. Comparison of finite element and discrete exterior calculus in computation of time-harmonic wave propagation with controllability. Journal of Computational and Applied Mathematics, 457, 116154, 2025.*

[¶] *M. Myyrä. Discrete Exterior Calculus and Controlled Time Integration for Time-Harmonic Acoustics. Submitted manuscript.*
M. Myyrä. Discrete exterior calculus and exact controllability for time-harmonic acoustic wave simulation. MSc Thesis, University of Jyväskylä, 2023.

CPU parallelization (MPI)

Meteor radar reflections in 3D

(EM scattering from plasmatic obstacles)

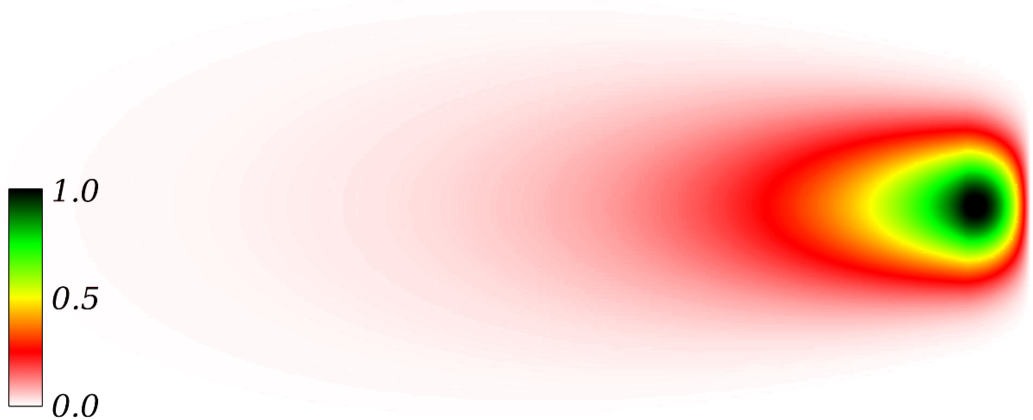

The normalized distribution of the meteor plasma frequency on the x-y-plane in a 10 m $\times 4$ m rectangle.

- Controlled time integration with DEC.
- Radar frequency $f_r = 300$ MHz.
- Simulations with computers *Paasikivi*, *Taito*, and *Sisu*.
- Reference line indicates the perfect parallelization.

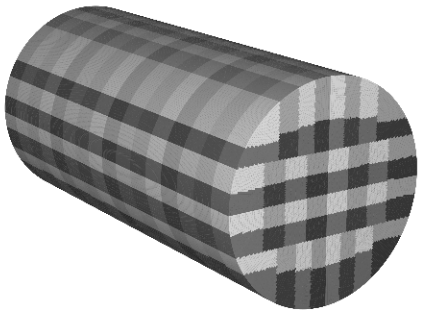

The mesh is divided into 1,024 blocks for the parallel computation.

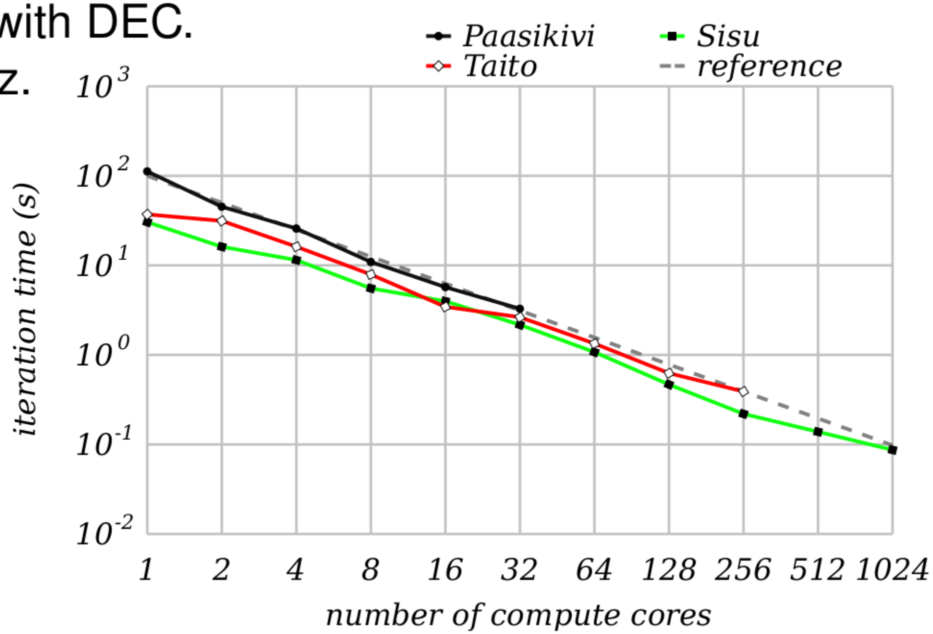

The iteration time by number of computer cores n. The reference line obeys function $t = 100\mathrm{s}/n$.

Computer	Processors	Available cores	Used cores
Paasikivi	Intel E7-8837 @ 2.67GHz	64 unreserved	32
Taito	Intel E5-2670 @ 2.60GHz	448	256
Sisu	Intel E5-2690v3 @ 2.60GHz	19,200	1,024

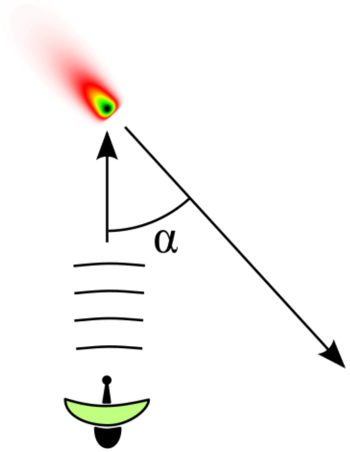

Propagation angle α.

J. Räbinä, S. Mönkölä, T. Rossi, J. Markkanen, M. Gritsevich, and K. Muinonen. Controlled time integration for the numerical simulation of meteor radar reflections. Journal of Quantitative Spectroscopy and Radiative Transfer, 178, 295–305, 2016.

DEC based controlled time integration was found to be more efficient than the volume integral equation (VIE) method and its performance is not sensitive to the level of discretization and the values of the material parameters.

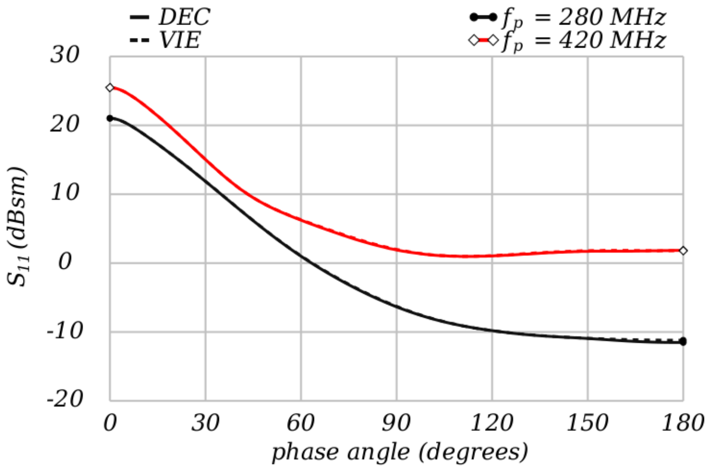

Phase functions at the maximum discretization levels.

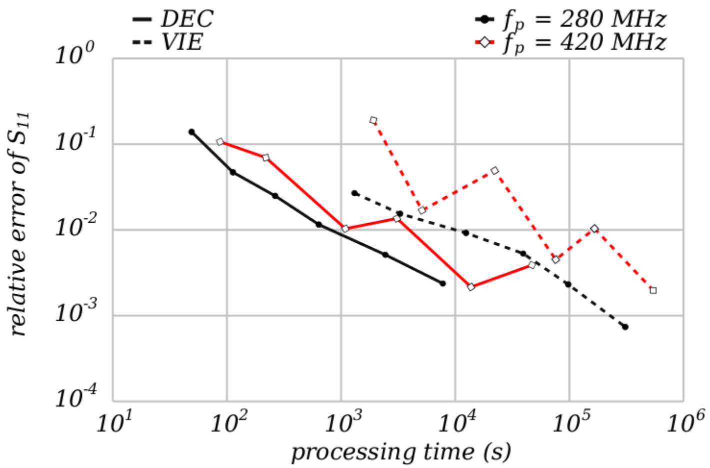

Relative error of component S_{11} by the simulation processing time.

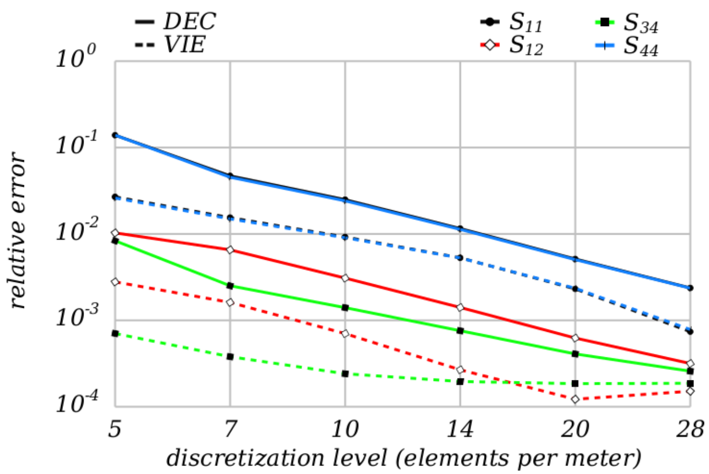

Relative errors of the Mueller matrix components, plasma frequency $f_p = 280$ MHz.

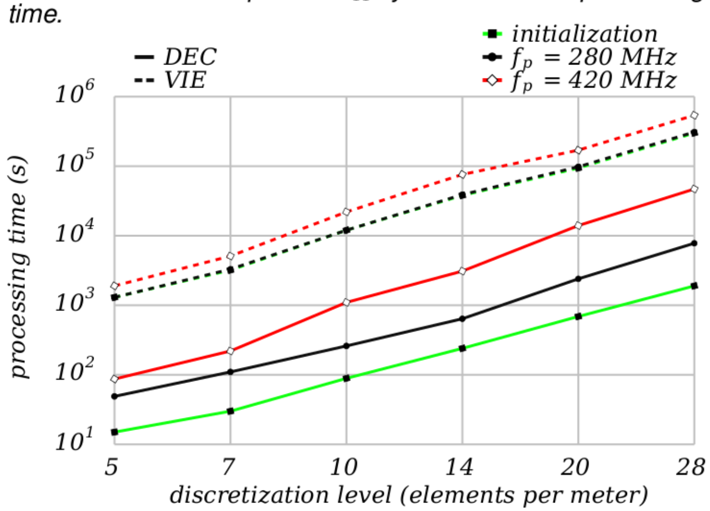

Processing times (s) for initialization and total simulation

GPU parallelization

The Gross–Pitaevskii equation

$$-\partial_t \hbar \star \Psi_R - \frac{\hbar}{2m}\mathrm{d}q_I = U_1\Psi_I + \sigma U_1 \mathsf{d} q_I,$$
$$\frac{\hbar}{2m} \star \mathsf{d} \star q_R - \partial_t \hbar \star \Psi_I = -U_8\Psi_R + \sigma U_8 \star \mathsf{d} \star q_R,$$

is a non-linear Schrödinger equation that models atomic Bose–Einstein condensates at ultra low temperature ($\sigma = 0$: original parabolic equation, $\sigma > 0$: hyperbolic equation).

Dynamics of vortex splitting

– The performance of the GPU implementation on one GPU corresponds to the performance of the CPU implementation executed on at least 60 CPU cores.

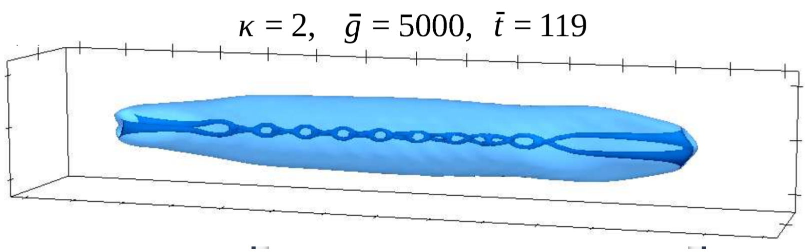

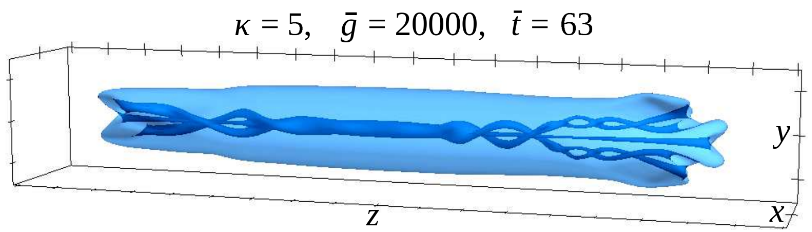

https://github.com/markus-kivioja/GpuDecGpe

M. Kivioja, S. Mönkölä, and T. Rossi. GPU-accelerated time integration of Gross-Pitaevskii equation with discrete exterior calculus. Computer Physics Communications, 278, 108427, 2022.

J. Räbinä, P. Kuopanportti, M. Kivoja, M. Möttönen, and T. Rossi. Three-dimensional splitting dynamics of giant vortices in Bose–Einstein condensates. Physical Review A 98 023624, 2018.

Alice ring

- Topological defect in a spinor Bose–Einstein condensate.

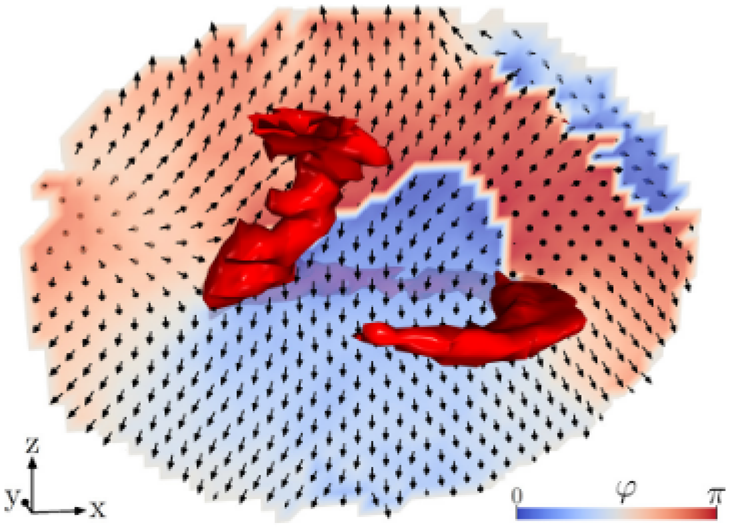

Alice ring breaking off at a single point.

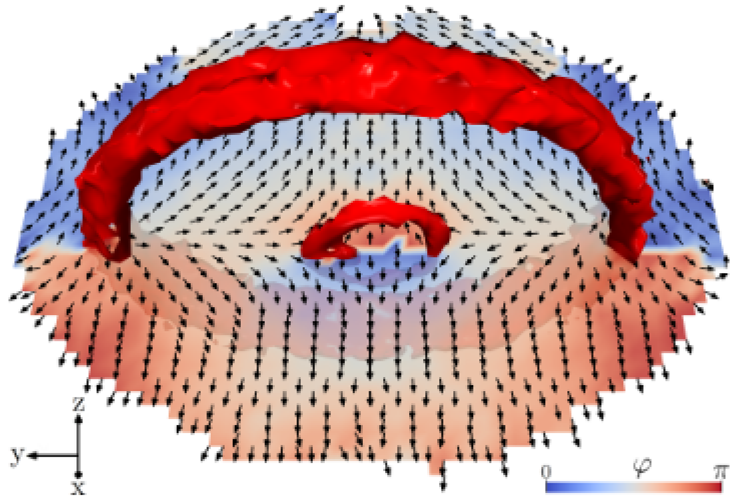

Coexistence of two Alice rings.

M. Kivioja, R. Zamora-Zamora, A. Blinova, S. Mönkölä, T. Rossi, and M. Möttönen. Evolution and decay of an Alice ring in a spinor Bose-Einstein condensate. Physical Review Research, 5(2), 023104, 2023.

Relativistic hyperbolic Gross–Pitaevskii equation

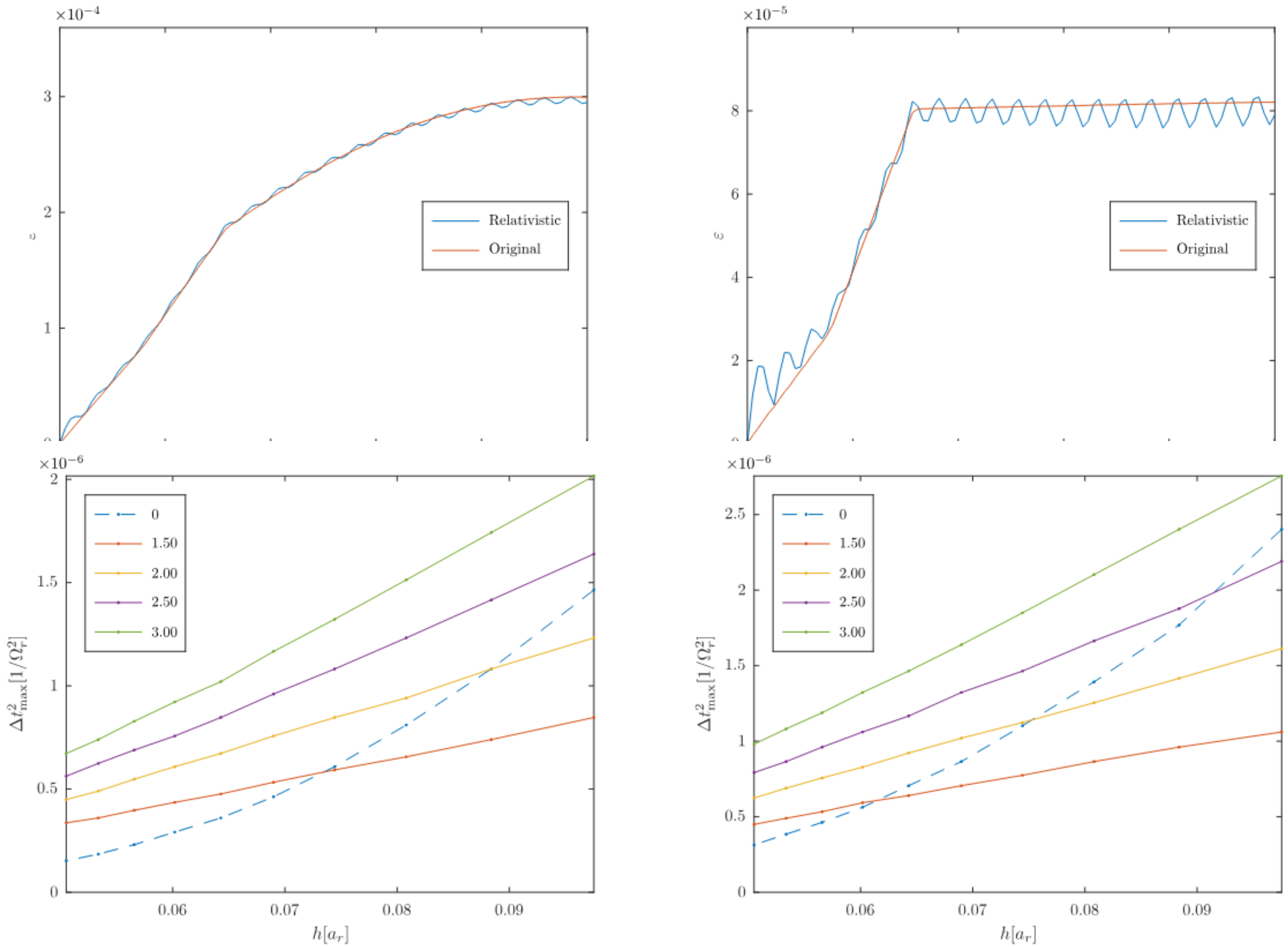

(a) Spin-1 GPE

(b) Spin-2 GPE

accuracy

stability ($\sigma = 0, 1.5, 2, 2.5, 3$)

M. Kivioja, S. Mönkölä, and T. Rossi. Hyperbolic spinor Gross-Pitaevskii equation for improved numerical stability, Manuscript in preparation.

Spacetime simulations

- All the metric properties, including the spacetime properties, are capsulated in the discrete Hodge operator.
- In spacetime, the mesh and spacetime stepping need to be constructed such that the causal relationships between events are preserved.

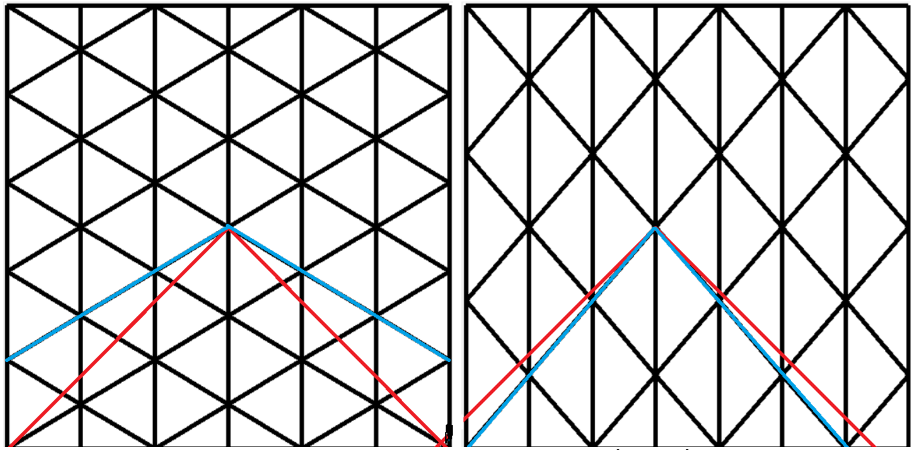

If the numerical domain of dependence (blue) is larger than the physical domain of dependence (red), the system is stable ("$c\Delta t < \Delta x$").

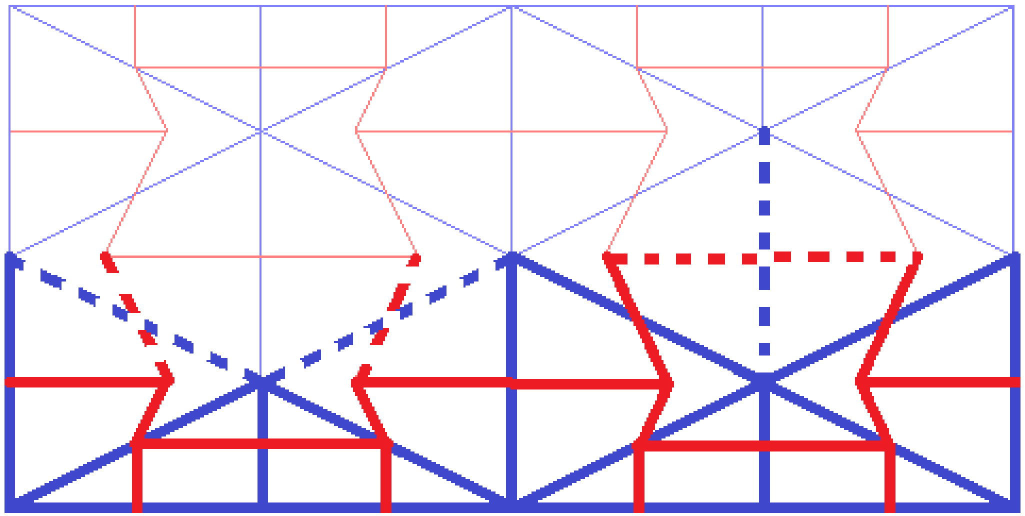

Spacetime stepping in (1+1)-dimensional primal (blue) and dual (red) grids.

(1+1)D

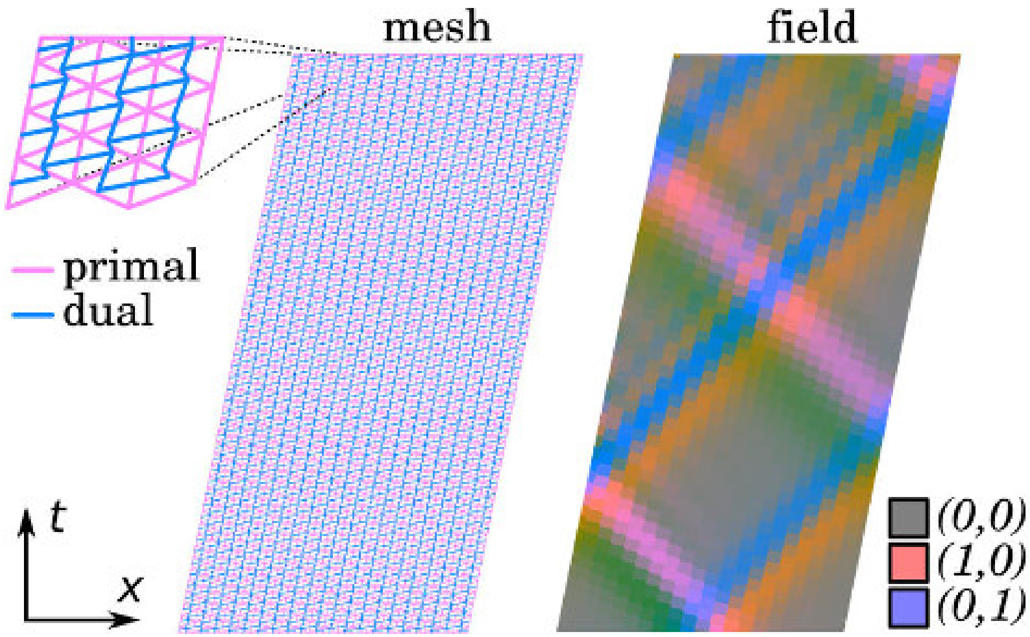

Uniform mesh, moving cavity (http://urly.fi/yNi).

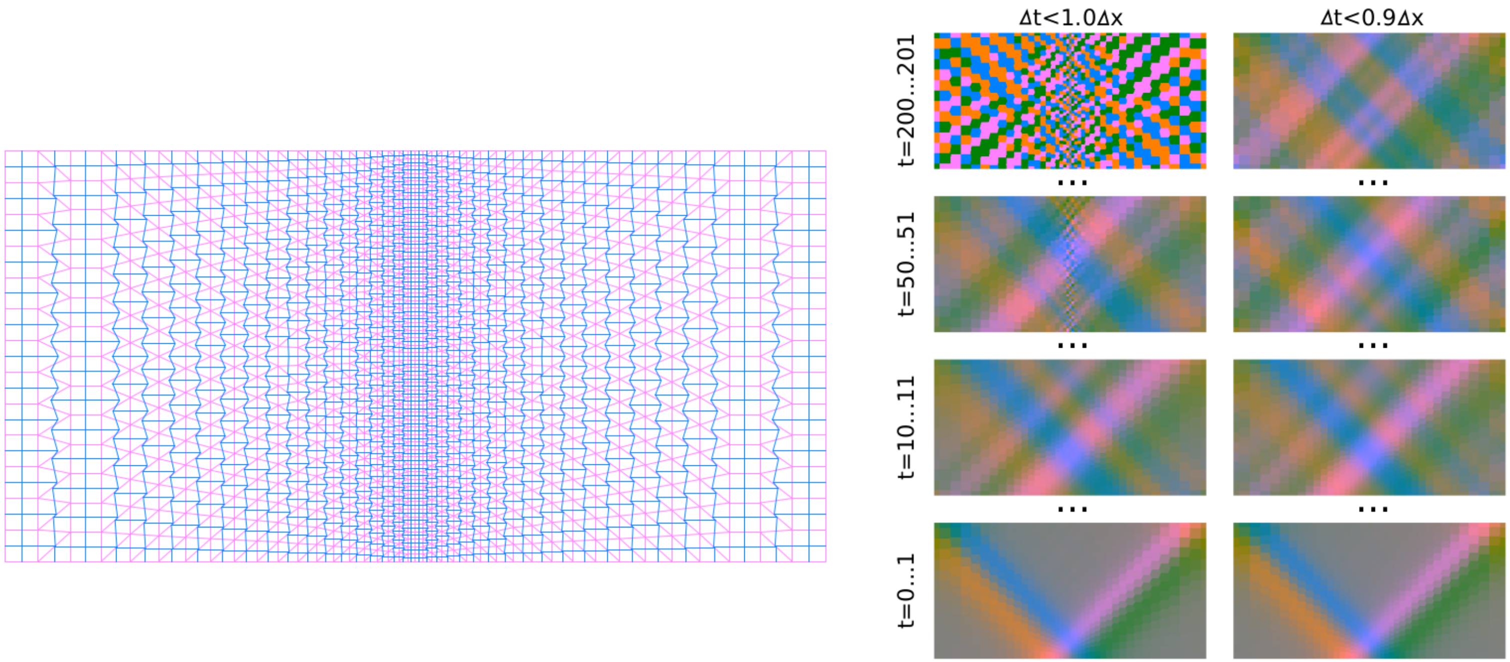

Continuous mesh refinement and stability test.

T. Rossi, J. Räbinä, S. Mönkölä, S. Kiiskinen, J. Lohi, and L. Kettunen. Systematisation of systems solving physics boundary value problems. In Numerical Mathematics and Advanced Applications ENUMATH 2019, 35–51, Springer, 2021.

(1+1)D

$$\partial_x E_t - \partial_t B_x = 0 \text{ in } [0,\pi]^2,$$
$$\partial_x B_x - \partial_t E_t = 0 \text{ in } [0,\pi]^2,$$

$$\begin{cases} B_x(x,0) = \sin(x), \\ B_x(0,t) = 0, \\ B_x(\pi,t) = 0, \end{cases}$$

$$\begin{cases} E_t(x,0) = 0, \\ E_t(0,t) = \sin(t), \\ E_t(\pi,t) = \sin(-t). \end{cases}$$

Uniform spacetime mesh

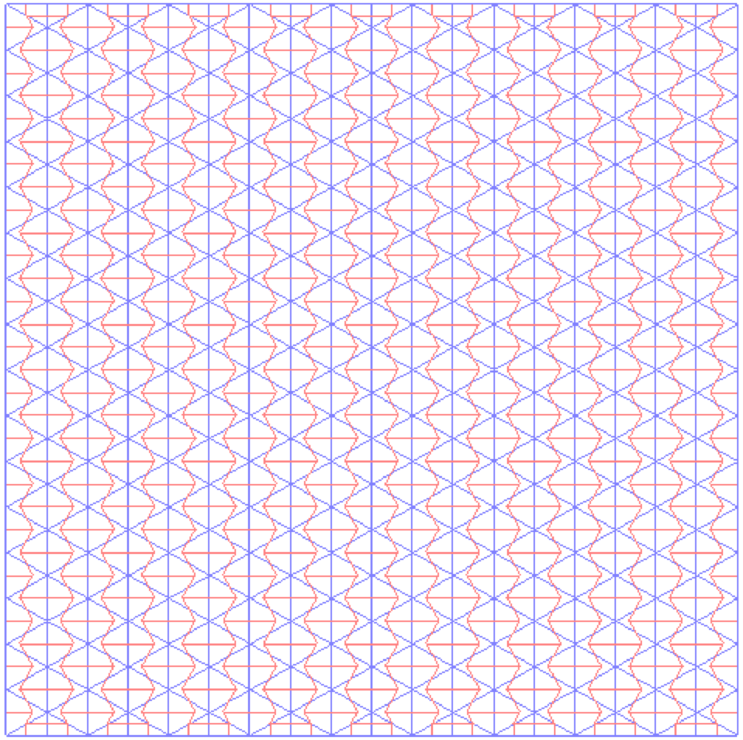

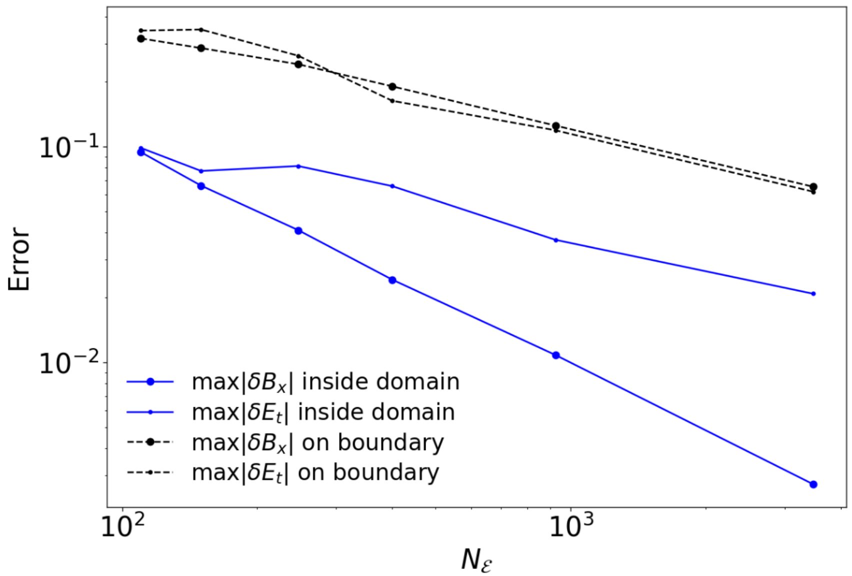

Continuous refinement

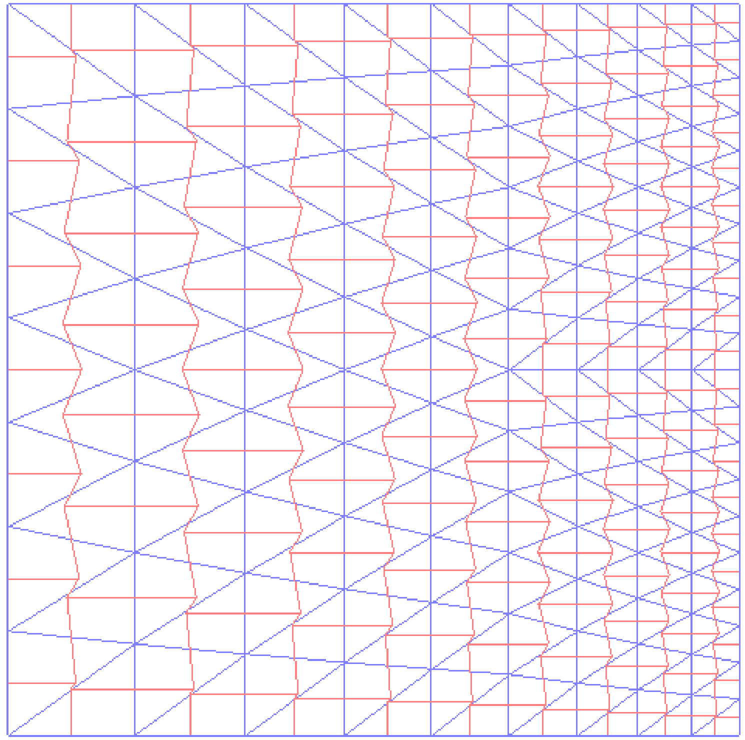

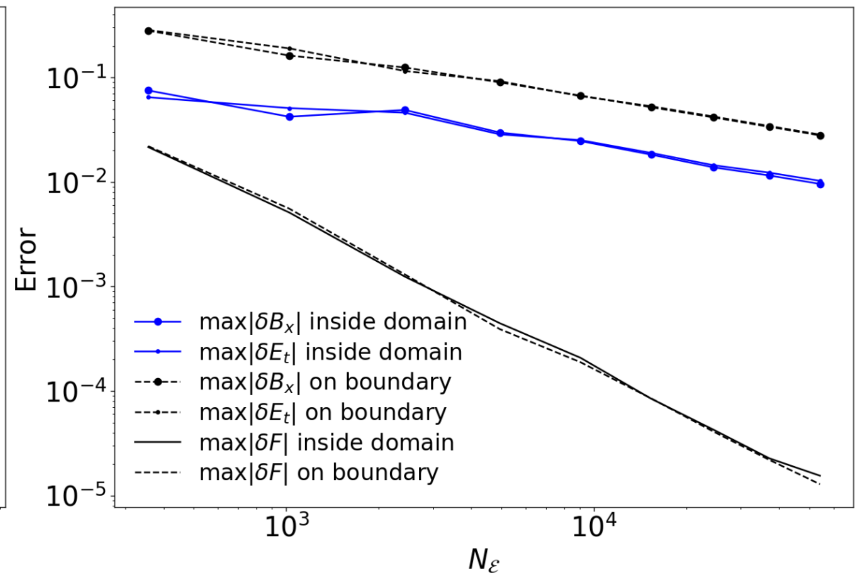

Maximum errors with respect to the number of edges.

J. Räty and S. Mönkölä. Local time-stepping for discrete exterior calculus on spacetime mesh with refinements. Journal of Computational Physics, 529, 113839, 2025.

(2+1)D

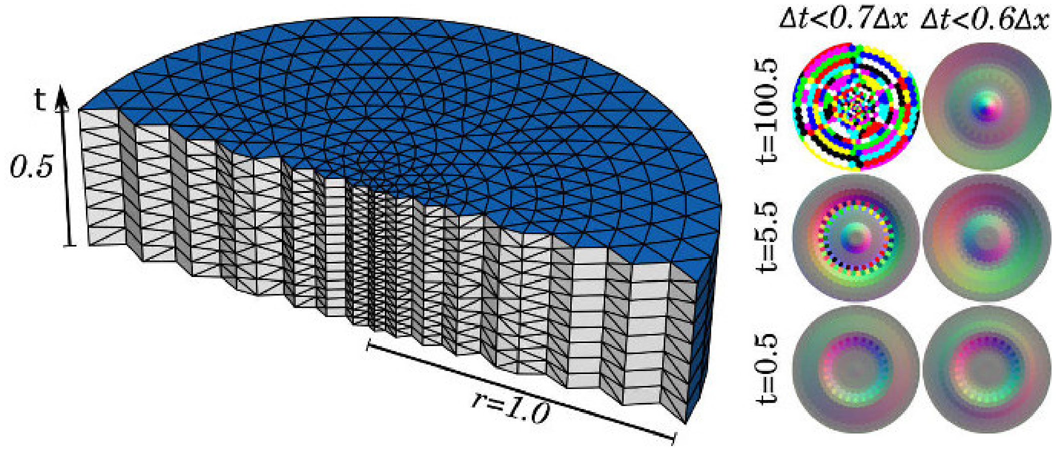

Mesh refinement in the center of the disc, stability test.

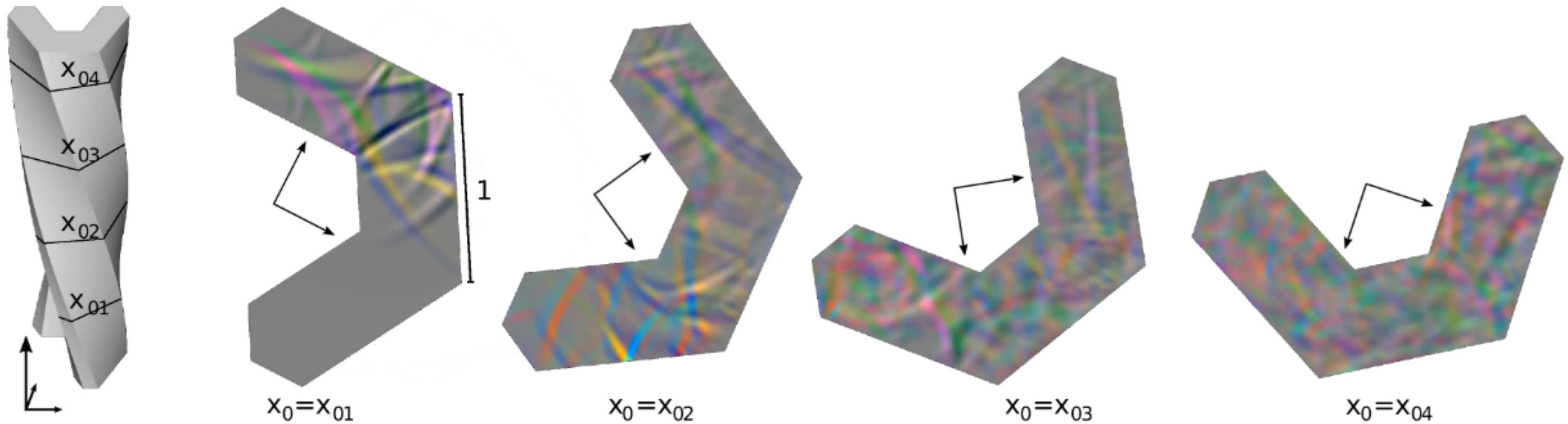

Spacetime grid twisted around the time axis (`https://urly.fi/1oxH`).

T. Rossi, J. Räbinä, S. Mönkölä, S. Kiiskinen, J. Lohi, and L. Kettunen. Systematisation of systems solving physics boundary value problems. In Numerical Mathematics and Advanced Applications ENUMATH 2019, 35–51, Springer, 2021.
S. Mönkölä, J. Räbinä, T. Saksa, and T. Rossi. (2+1)-dimensional discrete exterior discretization of a general wave model in Minkowski spacetime. Results in Applied Mathematics, 25, 100528, 2025.

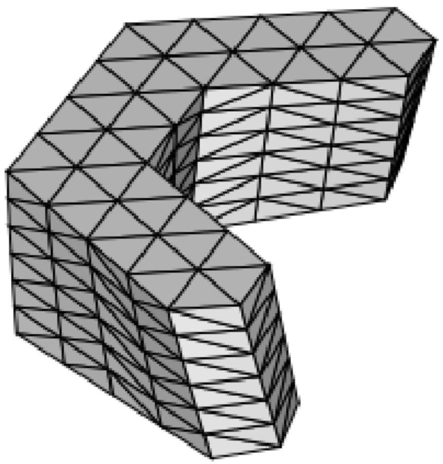

Synchronous time-stepping, constant time instants.

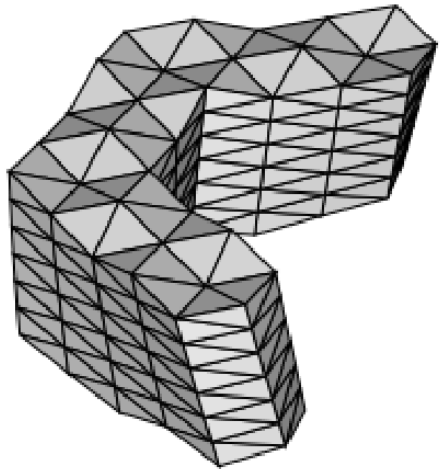

Asynchronous time-stepping, varying time instants.

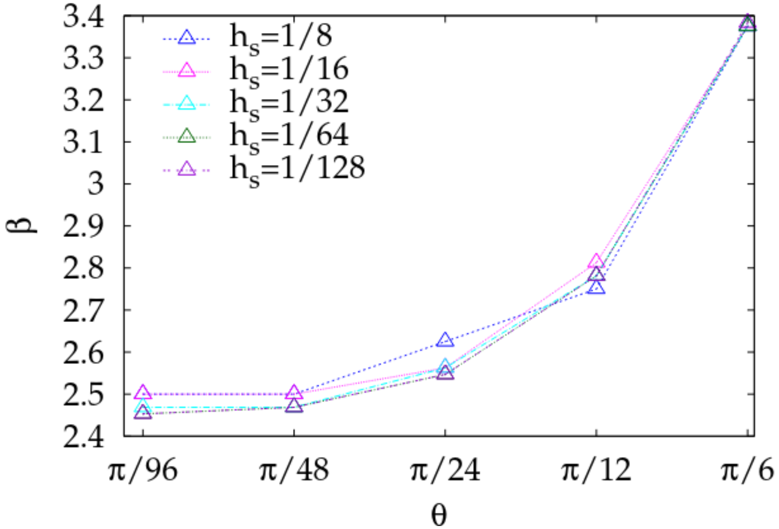

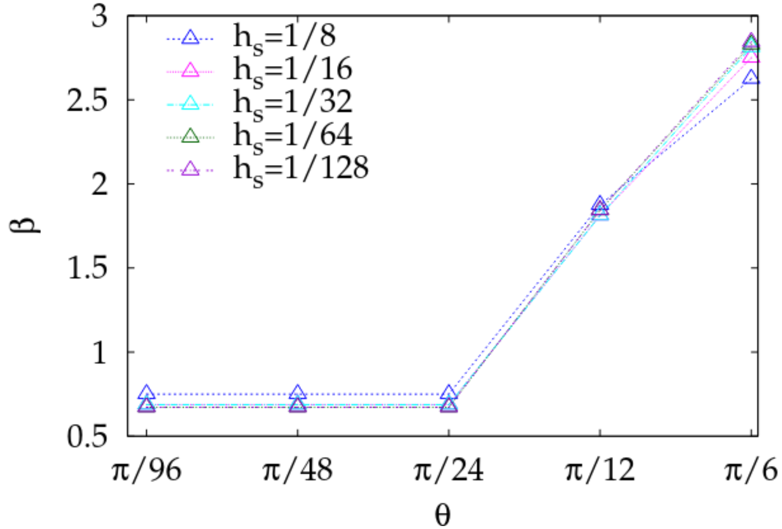

Stability factor β w.r.t rotation speed angle θ for several spatial mesh refinements with the largest stable timestep.

$$\Delta t < \Delta x / \beta$$

- The stability condition for asynchronous time-stepping is less strict than the stability condition for synchronous time-stepping.
- Constructing asynchronous time-stepping requires more computing time.
- Not a significant difference in CPU time requirements with the largest stable timesteps.

(3+1)D

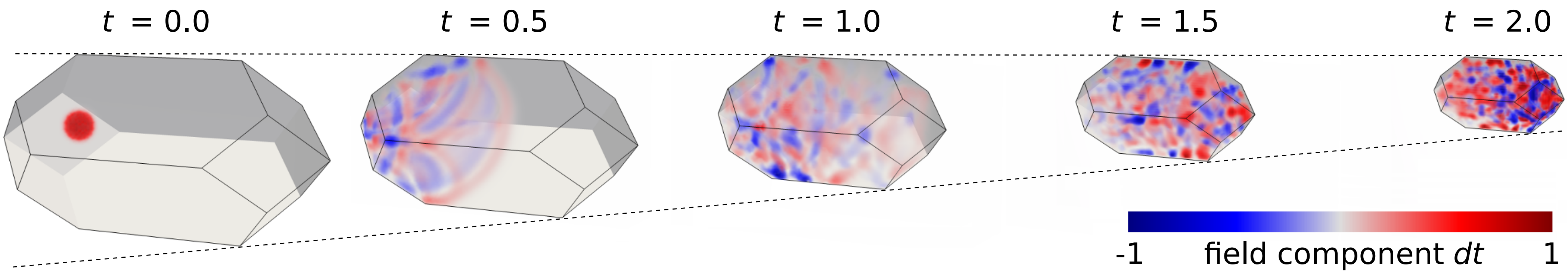

Shrinking domain (https://urly.fi/1oWx).

T. Rossi, J. Räbinä, S. Mönkölä, S. Kiiskinen, J. Lohi, and L. Kettunen. Systematisation of systems solving physics boundary value problems. In Numerical Mathematics and Advanced Applications ENUMATH 2019, 35–51, Springer, 2021.

Higher-order methods

- Require higher-order discrete Hodge operators. These are obtained using higher-order interpolants when the mesh is suitably created (start with an initial mesh and form a refinement containing certain “small cells”).
- Systematic approaches exist for simplicial and cubical meshes

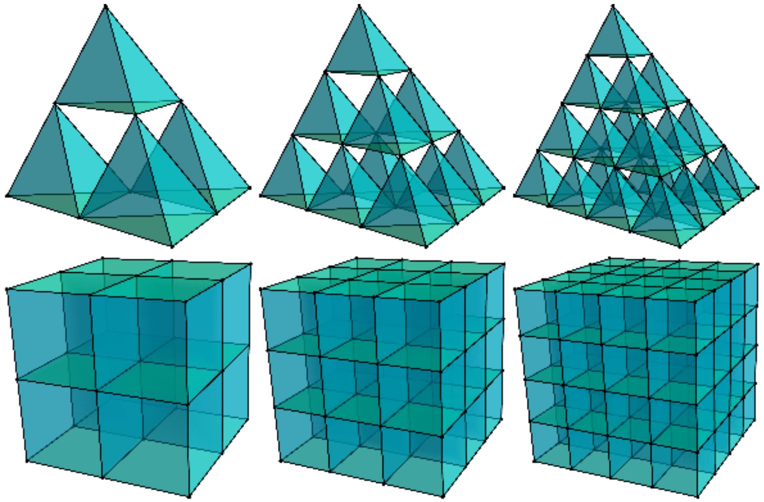

  - ”small simplices” of Rapetti and Bossavit‖,
  - ”small cubes” of Lohi **.

- Discrete differential forms (cochains) interpolated on the refined meshing higher-order finite element differential forms (Whitney forms or cubical forms).

‖Following the idea of mapping simplices to their so called homothetic images presented in *F. Rapetti and A. Bossavit, Whitney forms of higher degree. SIAM J. Numer. Anal. 47 (3) 2369–2386, 2009.*

**L. Kettunen, J. Lohi, J. Räbinä, S. Mönkölä, and T. Rossi. Generalized finite difference schemes with higher order Whitney forms. ESAIM: Mathematical Modelling and Numerical Analysis, 55(4), 2021.
J. Lohi. New degrees of freedom for differential forms on cubical meshes. Advances in Computational Mathematics, 49(3), 42, 2023.
J. Lohi. Higher order approximations in discrete exterior calculus. PhD thesis, University of Jyväskylä, 2023.
https://github.com/higher-order-dec/code

(1+1)D

The second order formulation $d \star du = f$.

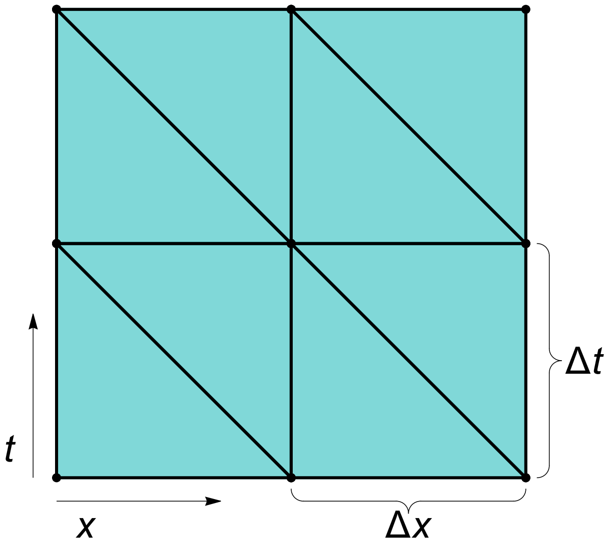

The type of the triangles used in the space-time mesh in domain $[0, 2] \times [0, 200]$.

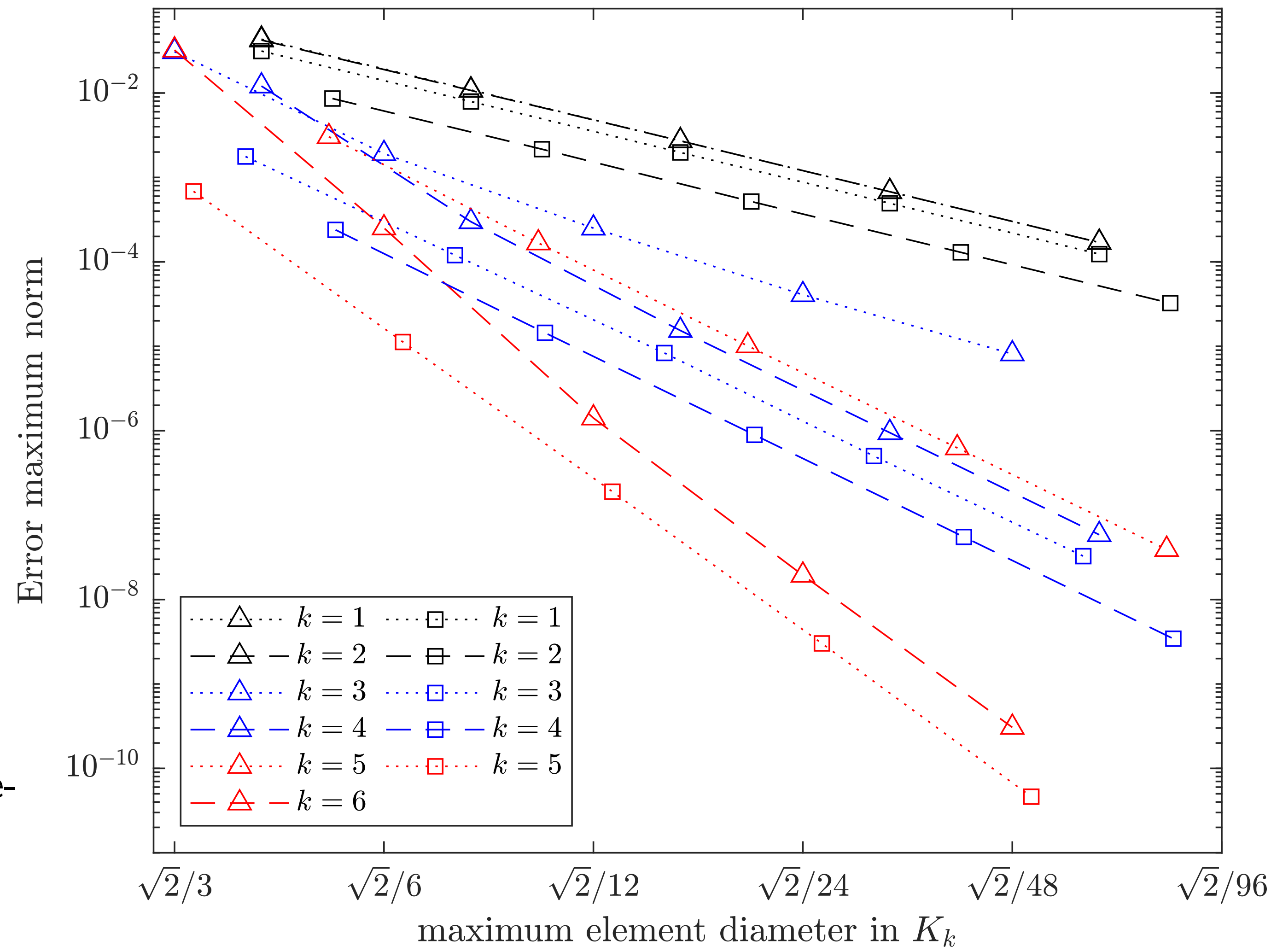

The results on triangular and square meshes with kth order approximations

(2+1)D

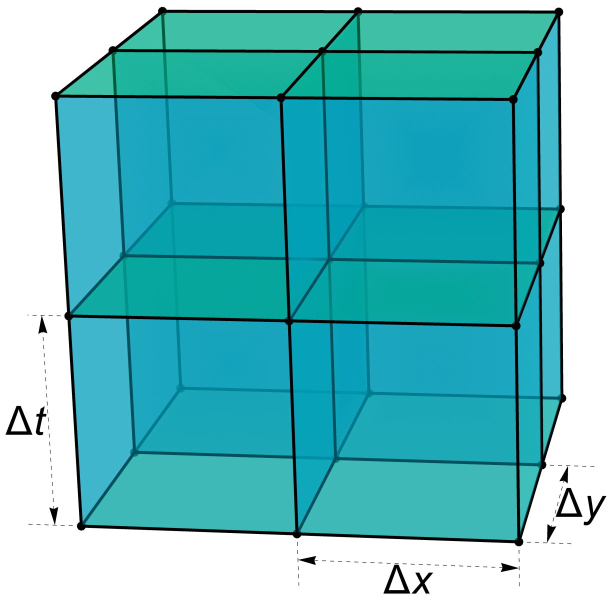

The type of the cubes used in the space-time mesh in $[0, 2] \times [0, 2] \times [0, 100]$.

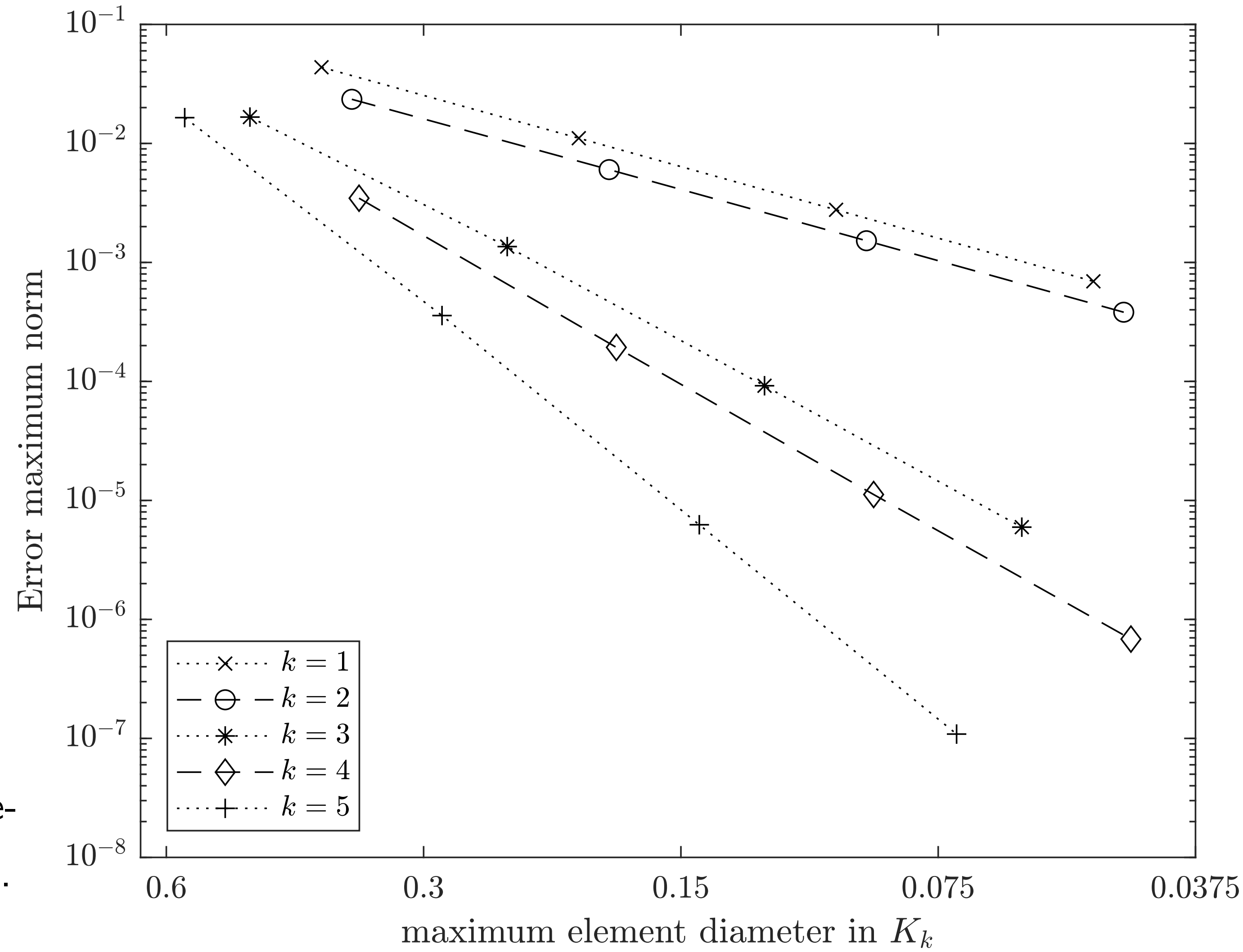

The results on cubical meshes with kth order approximations.

On-going/future work

A new implementation in the Rust programming language by Mikael Myyrä[††]

- Application areas:
  - nanoscale thermal transport in solids at very low frequencies,
  - magnetically confined plasmas in space/astrophysics (Maxwell-Vlasov equation).

Proof engineering in the interactive theorem prover Coq by Sampsa Kiiskinen [‡‡]

- Machine proofs for numerical mathematics.

[††] https://molentum.me/notes/dexterior/, https://codeberg.org/molentum/dexterior

[‡‡] *S. Kiiskinen. Curiously Empty Intersection of Proof Engineering and Computational Sciences. In Impact of Scientific Computing on Science and Society, 45–73, Springer, 2023.A-L. Erkkilä, J. Räbinä, I. Pölönen, T. Sajavaara, E. Alakoski, and T. Tuovinen. Using wave propagation simulations and convolutional neural networks to retrieve thin film thickness from hyperspectral images. In Computational Sciences and Artificial Intelligence in Industry, 261–275, Springer, 2021.*

Summary

- DEC has been successfully used in several disciplines, from classical to quantum mechanics.
  - Enables grid structures suitable for complex geometries.
  - Efficient time evolution by construction with diagonal discrete Hodge operator.
  - Higher-order methods improve accuracy at the expense of increased computational cost.
  - Exact controllability method provides a framework for solving time-harmonic problems.
    - Harmonic Hodge correction increases accuracy.
- General differential form model in spacetime
  - DEC is a natural discretization tool,
  - covers relativistic hyperbolic boundary value problems by nature,
  - parabolic and elliptic problems are simplifications,
  - space and time-stepping can be separated,
  - translates to various Clifford algebras.